HAL
open science

Structural Characterization of Hydrothermal Carbon Spheres by Advanced Solid-State MAS 13 C NMR Investigations

Niki Baccile, Guillaume Laurent, Florence Babonneau, Franck Fayon, Maria-Magdalena Titirici, Markus Antonietti

To cite this version:

Niki Baccile, Guillaume Laurent, Florence Babonneau, Franck Fayon, Maria-Magdalena Titirici, et al.. Structural Characterization of Hydrothermal Carbon Spheres by Advanced Solid-State MAS 13 C NMR Investigations. Journal of Physical Chemistry C, 2009, 113 (22), pp.9644-9654. 10.1021/jp901582x . hal-00393439

HAL Id: hal-00393439

https://hal.science/hal-00393439

Submitted on 3 Feb 2017

HAL is a multi-disciplinary open access archive for the deposit and dissemination of scientific research documents, whether they are published or not. The documents may come from teaching and research institutions in France or abroad, or from public or private research centers.

L'archive ouverte pluridisciplinaire **HAL**, est destinée au dépôt et à la diffusion de documents scientifiques de niveau recherche, publiés ou non, émanant des établissements d'enseignement et de recherche français ou étrangers, des laboratoires publics ou privés.

IMPORTANT NOTE : Please be aware that slight modifications occurring after Proof correction may occur between this version of the manuscript and the version on the Publisher's website----------

Structural Characterization of Hydrothermal Carbon spheres by Advanced Solid-State MAS ^{13}C NMR Investigations

Niki Baccile[1,2], Guillaume Laurent[2], Florence Babonneau[2], Franck Fayon[3], Maria-Magdalena Titirici[1], Markus Antonietti[1]* \

1-Max-Planck Institute for Colloids, Research Campus Golm, D-14424 Potsdam, Germany

2-UPMC Univ Paris 06 and CNRS, UMR 7574, Chimie de la Matière Condensée de Paris, F-75005, Paris, France

3-CNRS, UPR3079, CEMHTI - Conditions Extrêmes et Matériaux : Haute Température et Irradiation, F-45071, Orléans cedex 2, France and Université d'Orléans, Faculté des Sciences, Avenue du Parc Floral, BP 6749, 45067 Orléans cedex 2, France

RECEIVED DATE (to be automatically inserted after your manuscript is accepted if required according to the journal that you are submitting your paper to)

CORRESPONDING AUTHOR FOOTNOTE

* Corresponding Author. E-mail: niki.baccile@upmc.fr, Fax: +33 1 44 27 47 69

+ UPMC Univ Paris 06, Laboratoire de Chimie de la Matière Condensée de Paris, 4 place Jussieu, F-75005, Paris, France

ABSTRACT The local structure of carbon spheres obtained via the hydrothermal carbonization process is characterized by using a combination of advanced solid-state ^{13}C NMR techniques. Glucose was chosen as the starting product because it offers the possibility of ^{13}C isotopic enrichment and is regarded as a model compound for more complex polysaccharides and biomass, as reported in recent studies. A number of ^{13}C solid-state MAS NMR techniques (single pulse, cross polarization (CP), inversion recovery cross polarization (IRCP), INEPT, ^{13}C-^{13}C proton-driven magnetization exchange and ^{13}C-^{13}C double quantum-single quantum (DQ-SQ) correlation experiments) were combined to retrieve information about binding motifs and C-C closest neighbor relations. We found that the core of the carbonaceous scaffold is composed of furan rings cross-linked by domains containing short keto-aliphatic chains instead of otherwise expected graphene-type sheets, as mainly reported either for hydrothermal carbon spheres or for biomass-related carbons obtained by low-temperature (< 350°C) pyrolisis treatment.

KEYWORDS. Carbon, Biomass, Hydrothermal Carbonization, Glucose, ^{13}C solid-state MAS NMR, Double quantum NMR.

Introduction

In a series of recent publications[1 - 5] a sustainable approach to the synthesis of powders, mesoporous, or nanostructured carbon materials using biomass as starting product was presented: carbohydrates and raw biomass treated at relatively low temperatures (160 < T < 220 °C) in water in autoclave can provide a carbonaceous colloidal spheres and particles with roughly 60-70 w% carbon content. Different reasons motivated these works. Firstly, there is a need to explore new cheap and sustainable ways to obtain chemicals[6] and advanced functional carbon materials from sustainable raw materials to replace on the long run crude oil. Secondly, in case of a really cheap pathway and useful mass products, recycling the byproducts of farmed biomass would additionally

be a way to sequester significant amounts of CO_2, creating a material benefit at the same time. The way our group approached the topic was the use of hydrothermal synthesis between 180°C and 220°C to obtain carbon-based colloidal spheres[1,2,15], nanofibers[7,8] or sponge-like mesoporous carbons being meaningful as soil conditioner, ion exchange resins or sorption coals[3,5]. The synthesis proved to be feasible when glucose[2] is used or even when raw biomass materials like oak leafs and orange peals are taken[3]. In the first case, surface chemistry could also be modified by mean of hydrophilic[5] or hydrophobic coupling agents[9]. Along similar lines, the group of Clark showed that a slightly different approach using expanded starch could provide functional materials with disordered mesoporosity, which proved to be satisfactory as catalysts in the esterification of succinic acid[10,11].

In order to use the material for applications in catalysis, chromatography or as storage materials, it is evident that both a control of the chemistry behind the process and a satisfactory knowledge of the final material structure are of primary importance. In spite of the undoubted usefulness of the recent re-discovery of the hydrothermal process to obtain carbonaceous material, some basic work is still lacking as far as process of formation and final structure of the C-C-network are concerned. Some groups tried to investigate, directly or indirectly, the reaction mechanisms which transforms glucose first into its three times dehydrate intermediate, 5-hydroxymethyl-furfural-1-aldehyde (HMF)[12,13,14] and then subsequently to the carbonaceous scaffold[15,16] but a clear description of the final structure and, consequently, of the reaction path leading to the carbonaceous material is still missing. The amorphous nature and the intrinsic chemical complexity are the main drawbacks preventing an easy and full comprehensive structural study using common techniques, like XRD or infrared spectroscopy. Nevertheless, FT-IR and in some cases FT-Raman spectroscopy have been the most popular, easily accessible, techniques used to discriminate between various functional groups (C=O, C=C, aliphatic carbons) so far[3,14,15]. XPS was also used to identify the main carbon sites but the spectral resolution is often worse than the one obtained using vibrational spectroscopies[9]. Even ^{13}C solid-state NMR has already been tempted[4,14,15] but mainly to

complement other techniques. As for IR data, the resulting spectra only helped in the identification of the main organic functions. However, the rather good spectral resolution obtained on those hydrothermal carbons suggested that they deserved deeper investigation with more advanced NMR techniques.

Solid-state NMR studies on a large variety of carbonaceous materials, especially in soils and sediments, have already been performed, and a number of contributions have used ^{13}C NMR[17- 27] to identify chemical species and to refine carbon structures. The most common experiments use ^{1}H to ^{13}C cross polarization (CP) technique coupled to Magic Angle Spinning (MAS), which has the advantage of signal enhancement leading to reasonable acquisition times with respect to ^{13}C single pulse MAS NMR experiments. Unfortunately, quantification using CP is more challenging than in a single pulse experiment due to the more complicated spin dynamics. On the contrary, single pulse (SP) experiments, which are largely preferred to CP for quantification, are generally time-consuming. Extensive signal broadening coming from the potential presence of paramagnetic centers can also be a complicating factor, but this has not really prevented deep investigations of coals or chars by solid-state NMR[28]. Cross polarization at one single contact time is in general the fastest approach to obtain preliminary information about chemical composition. For improvement, Sullivan[18] presented CP experiments at variable contact times together with acquisition under modified CP conditions and two dimensional ^{13}C homonuclear magnetization exchange experiments to attribute large line widths to inhomogeneous broadening effects. Dela Rosa *et al.*[19] studied ^{1}H longitudinal relaxation times in the laboratory frame T_1 as well as in the rotating frame $T_{1\rho}$ and performed CRAMPS experiments on various coals to discriminate the presence of large amount of oxygenated sites. Finally, Tekely *et al.*[20] employed the ^{13}C transverse dephasing times T_2' to differentiate, based on proton mobility, aliphatic and aromatic components in overlapping signals.

We have recently found[29] by a combination of ^{13}C solid state MAS NMR and SEM that whatever the complexity of hexose carbohydrates (glucose, amylopectin or starch) used in the coalification

process is, the NMR response and in part the particle morphology of final carbons are very close, indicating the existence of a similar chemical coalification process in behind. Very similar ^{13}C NMR spectra of carbons have indeed also been reported by other authors both after hydrothermal treatment of starch[4] and fructose[15] and *also* from pyrolytic treatment at moderate temperatures (< 350°C) of a variety of biomass-derived sources like rice hulls[30], pectin[25], starch[31] or cellulose[32]. This is an important precondition to ensure that the structural study on carbon obtained from ^{13}C-enriched glucose reported in the present paper has broader validity. ^{13}C isotopic enrichment (which would be more demanding for complex biomass) is a requirement to enable a complete NMR study that combines advanced methods, as recently illustrated on the structural characterization of ^{13}C-labeled graphite oxide[33].

The goal of the present contribution is to show that hydrothermal carbon from ^{13}C isotopically enriched D(+)-glucose is a good model to analyze the chemical connection motifs of biomass-derived carbons obtained either via a hydrothermal or pyrolysis step at temperatures below 350°C. This goal is achieved by combining ^{13}C solid-state MAS NMR methods such as one-dimensional (single pulse, CPMAS, IRCP, through-bond C-H filtering -INEPT-), and two-dimensional experiments (^{13}C-^{13}C exchange spectroscopy and through space ^{13}C homonuclear double-quantum single-quantum correlation).

Experimental Section

Sample Preparation. For all samples, about 15 ml of a deionized water solution containing 10 wt% in mass of D(+)-Glucose (with the diverse isotope labeling discussed below) is sealed into a glass vial inside a typical PTFE-lined autoclave system for hydrothermal reaction at 180°C for 24h. After reaction, the autoclave is cooled down in a water bath at room temperature. The obtained black solid powder is then separated from the remaining aqueous solution by centrifugation (7000 rpm for 20 minutes) and dried at 80°C in a oven under vacuum during 12 hours. Non-enriched D(+)-glucose (Aldrich, CAS: 50-99-7), D-(+)-Glucose-1-(^{13}C) labeled at the C_1-position (Aldrich,

CAS: 40762-22-9) and fully labeled D-Glucose-$^{13}C_6$ (Aldrich, CAS:110187-42-3) have been used to prepare the samples that are listed in Table 1.

Table 1 Molar ratios of non-enriched, fully and selectively enriched glucose samples used in this study.

	Non-enriched D(+)-glucose	Partially enriched D-glucose-1-^{13}C	Fully enriched D-glucose-$^{13}C_6$
HC0	100	-	-
HC20	80	20	-
HC80	20	-	80

GC-MS experiments have been performed with an Agilent Technologies (GC= 6890N; MS= 5975) apparatus.

NMR experiments. Solution ^{13}C NMR experiments (acquisition with power-gated decoupling using a 30° flip angle) were performed on a Bruker Avance 400 MHz (9.4 T) spectrometer with a BBO gradient coil for 5mm tubes probe head.

^{1}H and ^{13}C solid-state MAS NMR experiments have been acquired on a Bruker Avance 300 MHz (7 T) spectrometer using 4 mm zirconia rotors spinning at a MAS frequency of ν_{MAS}= 14 kHz. ^{1}H and ^{13}C chemical shifts were referenced relative to tetramethylsilane (TMS; δ= 0 ppm).

Single pulse MAS experiments: pulse lengths (90° flip angle) for ^{13}C and ^{1}H were 3.15 and 3.80 μs and the optimum recycle delays were 30 s and 3 s, respectively. Two-pulse phase-modulated (TPPM) proton decoupling[34] was applied during ^{13}C acquisition (80 kHz). Number of transients was 4 for ^{1}H (all samples) and 64 for ^{13}C experiments (HC80). Spectra have been decomposed with DMFIT2004 software[35]. Integration values should be considered with a 10% error coming from a trial and error methodology used in the fitting procedure.

CP-MAS experiments: recycle delay for all CP experiments was 3 s and TPPM decoupling was applied during signal acquisition. Cross-polarization transfers were performed using adiabatic tangential ramps[36,37] to enhance the transfer efficiency with respect to other known methods[38] and

the CP contact time was t_{CP} = 3 ms unless otherwise indicated. NS = 1840 (HC0), 440 (HC20), 32 (HC80). All FIDs were subjected to an exponential multiplication (EM) function with a Line Broadening value of LB = 50 Hz prior Fourier transform

IRCP experiments: in order to get a complete spectral editing in CP MAS NMR, inversion recovery cross polarization (IRCP) is generally used. The principle of this sequence is reported elsewhere[39,40,41,42,43] and the only modification compared to the classical CP sequence is the introduction of a phase inversion during the contact time. ^{13}C transverse magnetization is firstly created during a relatively long contact time, t_{CP}, and is then progressively inverted during an inversion time, t_i. The dynamics of inversion is similar to the polarization dynamics in a standard CP sequence[44], and thus strongly depends on the ^{13}C-^{1}H dipolar coupling. This sequence is therefore very sensitive to the local proton environment and to molecular motion and a careful analysis of the CP dynamics allows a clear distinction between the various $^{13}CH_x$ sites depending on the x value and also between rigid and mobile $^{13}CH_x$ sites. The main advantage of this experiment relative to the standard CP sequence is that the magnetization starts from an optimum value, then decreases and eventually becomes negative when increasing t_i. It is thus easy to visualize differences in inversion dynamics of various signals especially when they overlap. On the basis of theoretical arguments, the relative rates of polarization are expected to be as follows:[45]

CH_3(static) > CH_2 > CH > CH_3(rotating), C(non-protonated)

For the IRCP experiments, a contact time t_{CP}= 3 ms was chosen in order to maximize the polarization of the ^{13}C nuclei, while 21 spectra were recorded for various inversion times, t_i, ranging from 1 μs to 5 ms. The recycle delays between pulses was 3 s and number of transient was 128.

INEPT experiments: Insensitive Nuclear Enhanced by Polarization Transfer (INEPT) experiments are commonly used in liquid state[46,47] to enhance the sensitivity of ^{13}C nuclei and to detect only protonated carbon sites and to edit them according to their specific J_{CH} coupling constants. Refocused INEPT experiments described in references[48,49,50] are more adapted to solid-state

samples since they allow to detect in-phase line shapes, avoiding cancellation effect in the case of broad ^{13}C resonances. In general, they reveal to be challenging when the proton resonances are subjected to a large homogeneous broadening due to strong ^{1}H homonuclear dipolar couplings. As clearly shown by Elena *et al.*[50], the presence of strong ^{1}H homonuclear dipolar interaction makes both the ^{1}H and ^{13}C transverse dephasing times very short in rigid organic solids and leads to a very weak efficiency of the refocused INEPT experiments. In such case, the use of a proton homonuclear dipolar decoupling sequence is required to minimize the transverse dephasing of coherences and to recover an efficient INEPT transfer.[50] In our case, the absence of ^{1}H homonuclear dipolar decoupling during the magnetization transfert and refocusing delay makes the efficiency of the experiment very low. The best INEPT efficiency obtained experimentally was below 5% of the theoretical maximum efficiency and was achieved using very short magnetization transfert and refocusing delays corresponding both to one rotor period ($\Delta 3 + \Delta 4 = 0.134$ ms). Therefore, the number of transients to record the refocused INEPT spectrum of our ^{13}C-enriched sample was almost 200 times higher (number of transient is 12600) than that of the single pulse MAS acquisition. For this experiment, the recycle delay was 3 s and TPPM decoupling was applied during signal acquisition.

Two-dimensional (2D) NMR:

- *CPMAS ^{13}C homonuclear double-quantum single-quantum (DQ-SQ) correlation experiments*. ^{13}C homonuclear DQ-SQ correlation spectra have been recorded at a spinning frequency of 14 kHz using the SC14 pulse sequence described in reference 51. Based on double quantum (DQ) dipolar recoupling between spin-1/2 nuclei, this experiment is a robust way to evidence the C-C atomic spatial proximities. We have employed the SC14 sequence[51] which requires a lower ratio of ^{13}C nutation frequency to spinning frequency (3.5) than other known DQ recoupling sequences like C7 [52], POSTC7 [53] or SPC5 [54]. Experimentally, this allows an efficient DQ excitation and reconversion with the use of a lower ^{1}H decoupling radio frequency field which should match almost 3 times the ^{13}C radio frequency field[54]. For this experiment, enhancement of ^{13}C signal was

obtained via a first CP step described above (t_{CP}= 3 ms) and followed by double quantum excitation (τ_E) and reconversion (τ_R) delays. Proton decoupling was applied both during DQ excitation and reconversion (continuous wave, ν_{1H}= 110 kHz) and signal acquisition (TPPM, ν_{1H}= 78 kHz). The type and amplitude of proton decoupling during DQ excitation and reconversion were finely tuned on both ^{13}C-glycine and ^{13}C-D(+)-glucose and were found to be coherent with what was already proposed in terms of DQ efficiency. The DQ excitation and reconversion periods were both set to 285.7 μs corresponding to two rotor periods. 16 t_1 increments with 304 scans each were collected and quadrature detection in the indirect dimension was achieved using the States method[55]. Exponential apodization with a line broadening factor of LB= 50 Hz was applied in both dimension prior Fourier transform.

- *CPMAS ^{1}H-^{13}C Heteronuclear Correlation (HETCOR).* Through-space heteronuclear correlation experiment between ^{1}H and ^{13}C have been performed using a standard 2D version of the CP sequence, detailed elsewhere[56]. Acquisition conditions for the CP experiment were given above. Here, 16 t_1 increments with 64 transients each were recorded and quadrature detection was achieved using the States method[55].

- *^{13}C-^{13}C proton-driven magnetization exchange spectroscopy*: ^{13}C homonuclear proton-driven magnetization exchange 2D spectra[57] have been recorded using a standard pulse sequence[58,59] in which ^{13}C transverse magnetization is created using standard single pulse excitation instead of classical CP step. The mixing time for ^{13}C-^{13}C proton-driven magnetization exchange was set to 150 ms. Proton decoupling was applied during both indirect t_1 and direct t_2 signal. 96 t1 increments with 32 transients each were recorded and quadrature detection in the indirect dimension was realized using the States method.

Results

GC-MS was performed in the liquid phase after different times of reaction, including the aqueous phase after 24 hours reaction time. The main component in all GC curves (results not shown) is a peak whose mass and fragmentation analysis suggests an attribution to hydroxymethylfurfural (HMF), the well-known dehydration product of glucose at high temperature[14,60,61,62,63]. Besides HMF, one finds at least 10 additional organic substances, the most prominent being levulinic acid, dihydroxyacetone and formic acid[63]. This result seems to be corroborated by the ^{13}C NMR spectrum analysis of the liquid phase of the extracted sample HC0 shown in Figure 1.

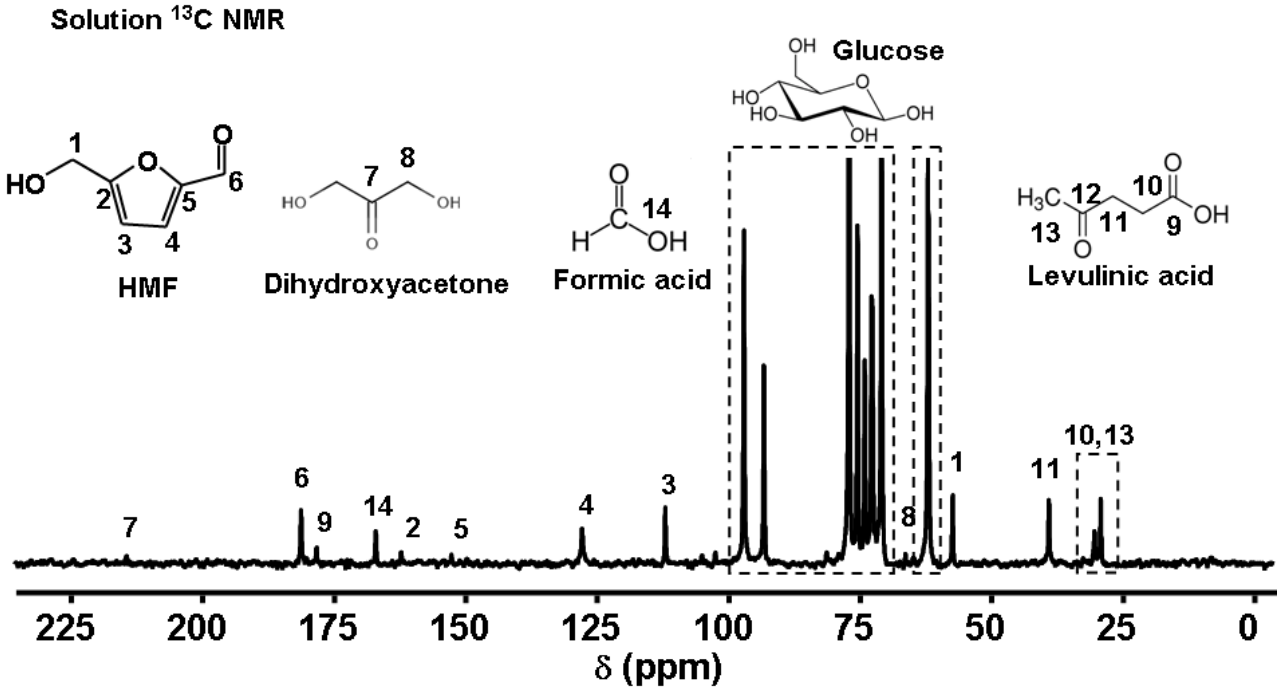

Figure 1 – ^{13}C solution NMR of extracted liquors after synthesis of HC0 sample (recycle delay= 2s; number of transient is 17138)

Two main sets of peaks are detected, and they can be indexed as follows[64]: signals labeled from 1 to 6 are attributed to HMF (C_6: 180.9, C_2: 161.8, C_5: 152.3, C_4: 127.3, C_3: 111.4, C_1: 56.5 ppm) as confirmed by ^{13}C NMR of the reference compound in D_2O (result not shown); peaks labeled from 9 to 13 are attributed to levulinic acid (C_9: 178.4, C_{11}: 37.8, C_{13}: 29.7, C_{10}: 27.9 ppm) while peak 14 (C_{14}= 166.2 ppm) is attributed to formic acid; both compounds are expected by-product of HMF dehydration, whose presence is abundantly detected in the liquors by GC-MS experiments[29]; traces of dihydroxyacetone (or related products) can also be identified by the carbonyl and methylene

peaks at, respectively, 214.5 and 65.3 ppm. Peaks in the 100-60 ppm region are attributed to unreacted glucose, even though their intensities (hence the amount of glucose) may vary from one reaction set to another. These findings support the general view that glucose first mainly dehydrates towards HMF, which on one side decomposes to form a mixture of mainly levulinic acid and formic acid[63,65] and on the other side reacts at high temperature to form the carbonaceous scaffold. Re-use of the aqueous phase in a second reaction under similar conditions resulted in further carbon phase formation and a complete elimination of the HMF peak.

The average chemical composition in weight-% of the resulting carbonaceous solids is C: 62 ± 3%, H: 4 ± 1%, O: 34 ± 3%, which corresponds to the following molar formula $CH_{0.77}O_{0.41}$. The large H content will be favorable to ^{1}H-^{13}C through-space (CP) or through-bond (INEPT) heteronuclear polarization transfer NMR experiments that will help in the identification of the various sites.

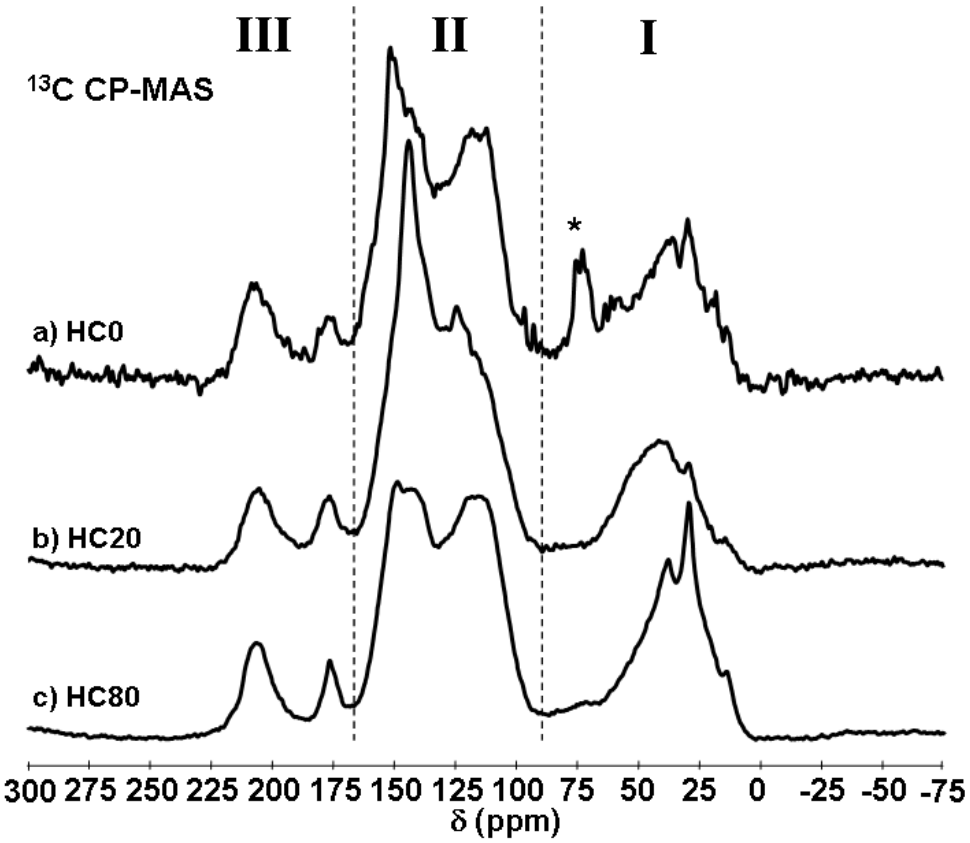

Figure 2 – ^{13}C CP-MAS NMR experiments of samples a) HC0, b) HC20, and c) HC80 obtained with contact time t_{CP} = 3 ms.

Figure 2 shows the ^{13}C solid-state CP MAS NMR spectra of hydrothermal carbon samples (Table 1) obtained from pure glucose (HC0), a mixture of pure and fully-enriched glucose (HC80) and a mixture of pure and selectively-enriched glucose-1-^{13}C (HC20) recorded using a contact time of 3 ms. A primary qualitative attribution based on literature[17-27] can be proposed for each spectral domain. Region I (0-100 ppm) is characteristic of sp^3 carbon atoms indicating the presence of a broad distribution of CH_x (X= 1, 2, 3) sites. Region II (100 to 160 ppm) is characteristic of sp^2 carbon atoms in C=C double bonds with signals between 140 and 160 ppm more specifically due to oxygen bound, O-<u>C</u>=C, sp^2 carbons. In region III (170-225 ppm), C=O groups either in carboxylic acid moieties (175 ppm) or ketones and aldehydes (200-220 ppm) resonate. Finally, a peak at 75 ppm, whose intensity largely varies among all materials, corresponds to residual glucose, as also compared to the large amount of residual glucose in the solution phase.

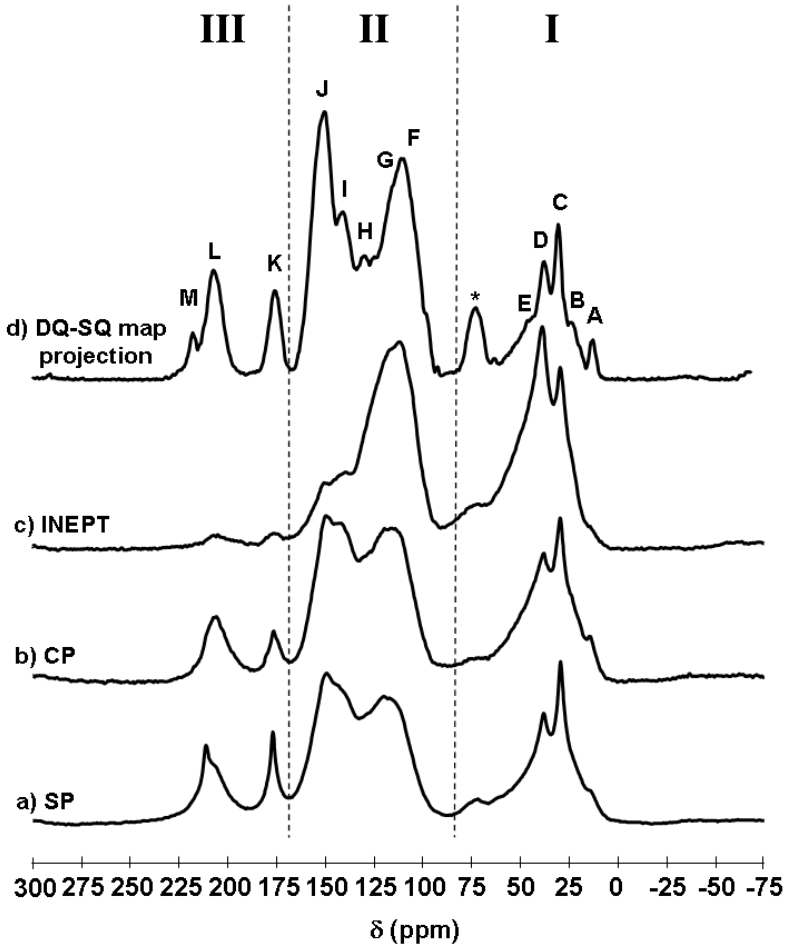

Figure 3 – ^{13}C MAS NMR spectra of sample HC80 recorded with various sequences: a) SP, b) CP and c) INEPT. d) Skyline projection of the 2D ^{13}C-^{13}C DQ-SQ experiment shown in Figure 6.

To contribute to a better understanding of the reaction mechanism, which transforms glucose into functionalized carbonaceous powders, selectively ^{13}C-enriched glucose molecule in position 1 (sample HC20) was used to promote amplification of specific signals especially in the carbonyl region, as known from previous works[60]. However all spectra (Figure 2) look similar, which demonstrates that the ^{13}C, initially in position 1, was abundantly reshuffled through the complete monomer structure or reacting sub-species. Even if a closer observation of the spectra nevertheless shows some slight differences in the relative intensities of several peaks, we exclude at the moment the employment of specific isotope labeling for a more refined investigation of the chemical condensation mechanism. However, as expected, comparison between HC0 (acquisition time:

5500s) and HC80 (acquisition time: 70s) shows that isotopic enrichment is extremely useful in terms of sensitivity. In addition, despite the high level of enrichment, peak broadening due to ^{13}C homonuclear dipolar couplings is not observed, showing that a MAS rate of 14 kHz is sufficient to efficiently average out the ^{13}C homonuclear dipolar interactions, which are expected to range between 2 and 7 kHz depending on C-C distances.

Such a high quality response allowed recording quantitative single-pulse (SP) MAS experiments on HC80 sample (Figure 3a). Very few differences can be noticed when comparing the SP to the CP-MAS spectrum recorded with a long contact time of 3 ms (Figure 3b), due to the large proton content (H/C = 0.77) and the presence of strong ^{1}H homonuclear dipolar coupling giving rise to efficient ^{1}H spin diffusion processes. Slight differences are mainly concentrated in the C=O region, where the two signals around 176 and 210 ppm are clearly multi-components: 1) a sharp peak centered at 210.0 ppm is present in the SP spectrum but hardly detected by CP; 2) similarly, the signal at 176.5 ppm in the SP spectrum reveals the presence of a sharp peak overlapping a broader signal. The origin of these resonances is very peculiar and it will be explained in the discussion section.

It is clear so far that ^{13}C NMR spectra suggest a complex nature of the final hydrothermal carbon with the presence of a larger variety of carbon sites. In the following, the ^{13}C resonance assignments have been refined combining several ^{13}C NMR techniques. INEPT technique gives a straightforward interpretation on protonated carbon sites, as carbon signals are filtered via the through-bond J-coupling. Cross-polarization experiments have been performed at different contact times ranging from 35 μs to 7 ms. We have found that this approach provides selective pieces of information mainly in region II characteristics of aromatic peaks. IRCP experiments were also performed at several inversion times (from 1 μs to 500 μs) and they were extremely useful in the spectral resolution of the complex multi-component aliphatic region. Finally, the 2D ^{13}C-^{13}C DQ-SQ correlation spectrum was very powerful to finely resolve most of the carbon species and to establish their connectivities. Our indexation (peaks A-M in Figure 3d and Table 2) is based on this

2D DQ-SQ correlation experiment (both using the skyline projection and the cross-peaks) and all techniques cited above; the decomposition of the skyline projection is shown in Figure 1 ESI. A detailed description of each experiment used to investigate the structure of the carbonaceous material is given in the following paragraphs.

Insight on protonated carbons by INEPT experiments. As shown in Figure 3c, definite proof of the identification of protonated carbon sites is provided by the refocused INEPT MAS experiment which allows probing ^{1}H-^{13}C through-bond (J-coupled) connectivities. Nevertheless, this experiment confirms the existence of protonated carbons in region I (10-50 ppm) as well as for the broad signal between 110 and 130 ppm (sp^2 sites), and demonstrates that majority of the sites contributing to the signal centered at 150 ppm are actually non-protonated. This is an important piece of information since it strongly suggests that the signals at 110-130 and 150 ppm can be mainly assigned to furanic O-C=<u>*C*</u>H- and O-<u>*C*</u>=CH- sites, respectively: indeed, similar chemical shift values are observed for α-positions (161.8 and 152.3 ppm, see Scheme 1) and β-positions (111.4 and 127.3 ppm, Scheme 1) in HMF, as shown in Figure 1b. In agreement to the known chemical steps which transform glucose into HMF, we believe that this compound reacts further so that the furan ring may constitute the majority of the carbonaceous scaffold, in agreement with CP, IRCP and DQ-SQ experiments shown later. Finally, the two low-intensity signals at 176.5 and 208 ppm suggest the presence of a small amount of aldehydes with respect to typical non-protonated carbonyl sites detected in the same chemical shift range, such as ketones and carboxylic acids, and indicating the aldehyde as a preferred reaction site. Nevertheless, the presence of residual aldehyde groups was also proved by ^{1}H-^{13}C CP HETCOR experiments performed at relatively short contact time of 500 μs (result not shown) showing a correlation peak between the C=O signal at 176.5 ppm and a proton resonance at ~9.0 ppm. One should remark that no cross peak was detected at 211.0 ppm, corroborating the CP data and confirming the assignment of this signal to a ketone group.

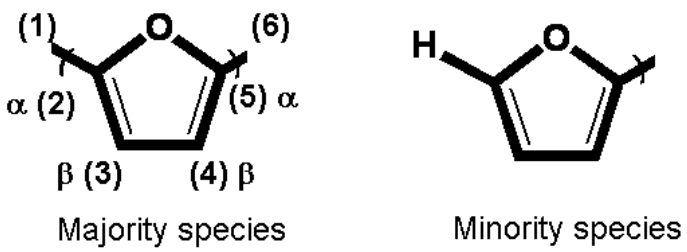

Scheme 1 . The furan ring with the α-position (or positions 2;5) and β-positions (or positions 3;4) highlighted

Insight on aromatic carbons using {^{1}H}-^{13}C CP experiments. Figure 4a shows {^{1}H}-^{13}C CP MAS spectra recorded at various contact times from very short (t_{CP}= 35 μs) to long values (t_{CP}= 10 ms). The spectrum recorded at t_{CP}= 35 μs mainly reveals aliphatic and β-carbons and looks very similar to the INEPT spectrum. This is expected since for short contact time magnetization transfers only occur across strong dipolar couplings corresponding to short C-H distances characteristic of C-H_x bonds.[66] The aliphatic zone (10-80 ppm) of the CPMAS spectra shows a very complex shape composed of several unresolved resonances for which more insight will be provided by the IRCP experiments in the next section. However, interesting insights can be actually gained in the aromatic region (100-160 ppm, region II). Five main peaks (F, G, H, I, J) are evidenced and the corresponding evolution of the integrated area of peaks (F), (G), (J), (I) as a function of cross polarization time is shown in Figure 4b (refer to Figure 2-ESI for some CP spectra decompositions at different t_{CP} values). Interestingly, peaks (G), (I), (J) show the same polarization behavior, typical of a quaternary carbon (as compared to the behavior of the ketone (L)-peak at 208 ppm, reported on the graph for comparative purposes), while peak (F) shows a very fast increase in intensity, which is typical of a protonated carbon. Therefore, CPMAS experiments clearly show that peak (G), which was expected to have a similar chemical nature as peak (F) on the basis of their very close ^{13}C chemical shifts, could not be assigned to protonated carbon as peak (F) and is dominated by quaternary species. We will use this important piece of information to depict the exact nature of the carbon sites related to peaks (F) and (G) after the analysis of the 2D DQ-SQ map. One important remark: CP behavior of peak (H) at 131.2 ppm reveals to be typical of a quaternary carbon (not

shown). This piece of information will provide valuable insights about the nature of this resonance in conjunction with the DQ-SQ experiment.

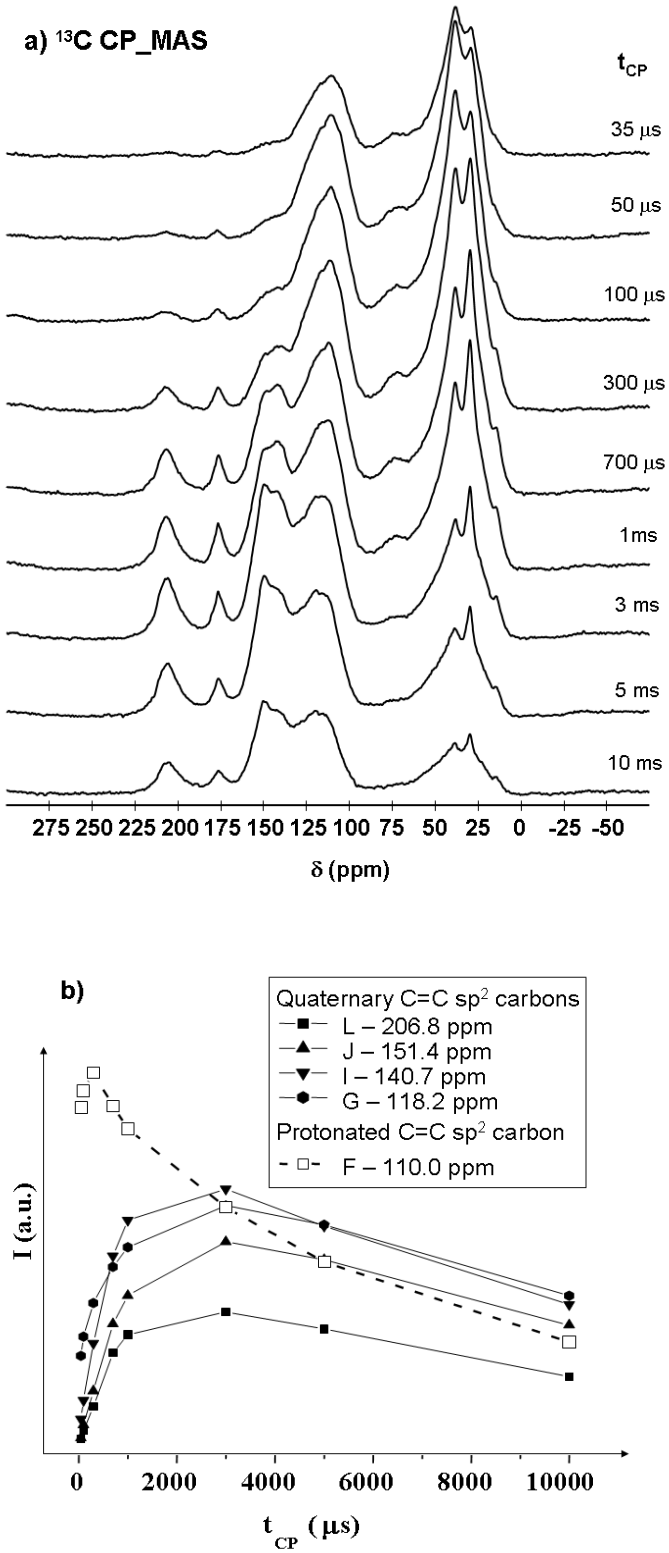

Figure 4 - Evolution of ^{13}C CP-MAS spectra recorded on HC80 for different contact times (a) and variation of peak intensities of aromatic region (b) as a function of the contact time

Insight on the aliphatic region using {^{1}H}-^{13}C IRCP experiments. For a detailed and complete analysis of the aliphatic region where a strong overlapping of signals is observed, IRCP is a better approach than simple CP-MAS. As highlighted in the experimental part, IRCP experiments are generally selective to rigid CH_2 and CH sites as their normalized intensity signal tends, respectively, to a negative value (-1/3) or to zero as a function of t_i. On the contrary, signal of mobile CH_3 and/or quaternary carbons remains positive. Figure 5a shows some IRCP experiments for the aliphatic region at selected inversion times; after 100 μs, the broad signal inverts exception made for two sharp components within peaks at 29.6 and 38.3 ppm. Decomposition of IRCP spectra is shown in Figure 3-ESI; typically, the set of peaks (A-E) from DQ-SQ projection (Figure 1-ESI) was used for some selected IRCP spectra. Finally, the evolution of the integrated normalized intensity as a function of the inversion time for some peaks is presented in Figure 5b. Negative intensity values occur for CH_2 groups whose peaks are at 23.9 (B), 28.7 (C) and 38.3 (D) ppm; stars shows the typical behavior for mobile CH_3 species, as confirmed for peak (A) at 13.9 ppm and sharp peak (C) at 29.6 ppm belonging to CH_3 groups; finally, intensity variation for peak (E) at 50.5 ppm shows the expected behavior for CH groups, as also confirmed by comparison to the behavior of the peak labeled (*) due to the CH of glucose (73.4 ppm), and acting as an internal CH standard. Table 2 summarizes the main families of CH_x groups (peaks A through E) but one should notice that peaks (C) and (D) are certainly multi-components, as resulting from the DQ-SQ projection (Figure 1-ESI) and the cross-peaks in the 2D map (next section).

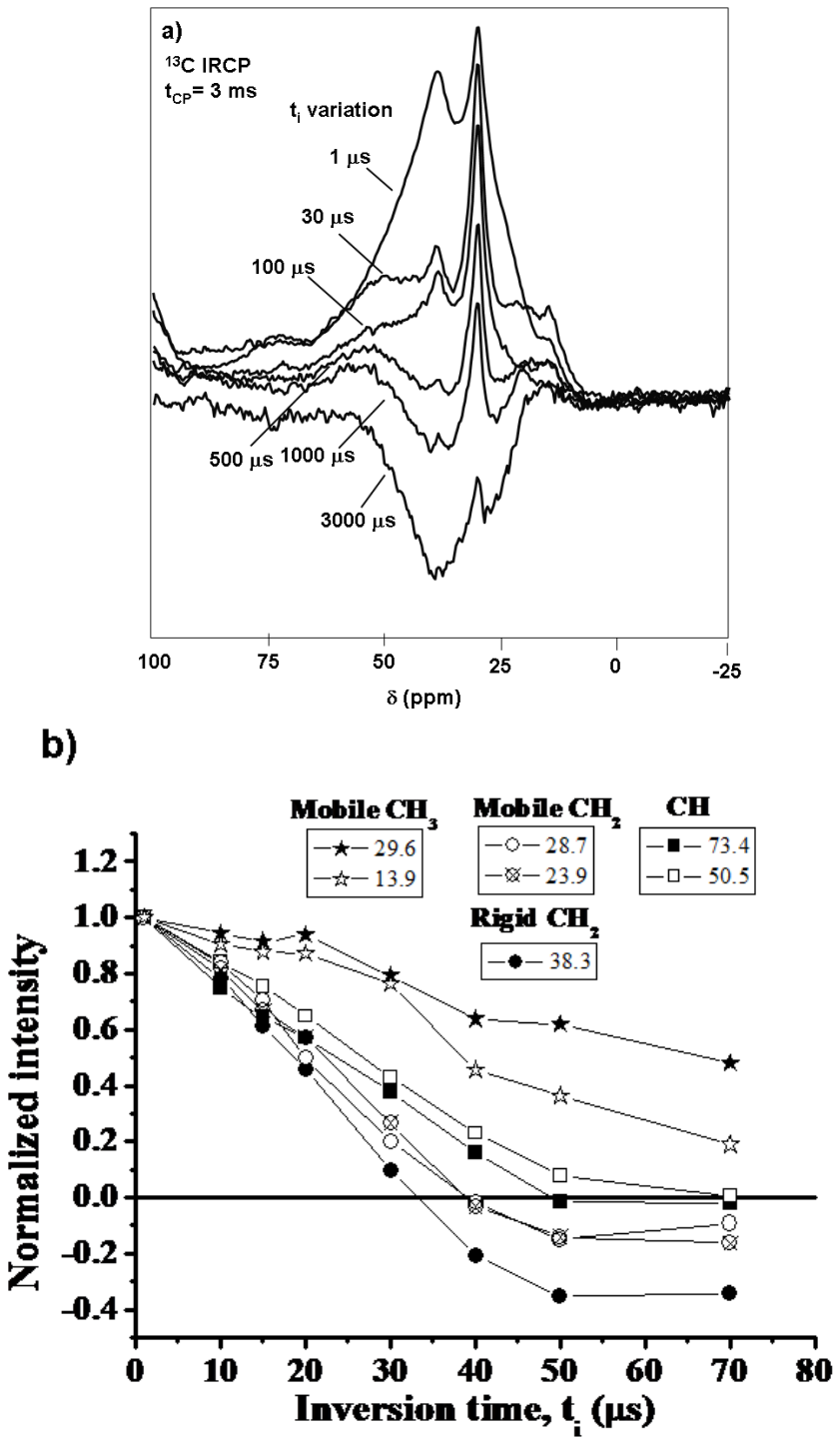

Figure 5 – a) IRCP spectra recorded at various inversion times in the aliphatic region for sample HC80; b) evolution of IRCP peak intensity for selected decomposed peaks belonging to various CH, CH_2 and CH_3 groups.

Table 2 – Peak assignment for HC80 material after decompositions of: ^{13}C DQ-SQ experiment, CP and IRCP experiments. Percentage of each carbon group was obtained by decomposition of HC80 SP spectrum. Quantitative data only concerns carbonaceous material, not including embedded levulinic acid (see text for explanation). Remaining 4% is attributed to residual adsorbed glucose (* peak at 73.4 ppm).

Spectral domain		CP/IRCP	INEPT	Peak	$\delta(^{13}C)$ (ppm)	Percentage %
I sp^3 C		Mobile CH_3	CH_x x= 1-3	A	13.9	23
		Rigid CH_2		B	23.9	
		Rigid CH_2		C	28.7	
		Mobile CH_3		C	29.6	
		Mobile CH_2		D	38.3	
		CH		E	50.5	
		CH		*	73.4	
II sp^2 C	β-C	CH	CH_x	F	110.0	29
		C		G	118.2	
				H	131.2	
	α-C	C	C	I	140.7	35
				J	148-156	
III C=O		-	CH_x	K	175-179	4
		-	C	L	202-207	9
				M	218.4	

Insight on spatial connectivity using ^{13}C homonuclear DQ-SQ correlation experiments. The experiments previously performed allowed identification of the different functions present in the carbonaceous samples but did not provide information about close spatial proximities between the various carbon groups. Indeed, several NMR methods exist to visualize short-range connectivities either via through-bond or through-space techniques: for example, the group of Emsley used double quantum excitation (INADEQUATE[67]) to probe carbon-carbon connectivities in biomass[68] while a recent report used a fpRFDR[69] pulse sequence to study ^{13}C-labelled graphite oxide[33]. For our study, we strongly preferred the use of double quantum excitation; in fact, the signals lying on the diagonal in a 2D DQ-SQ experiment provides crucial pieces of information about connectivity among equivalent sites. Since we were unable to optimize a high quality INADEQUATE

experiment on our samples, probably due to the low values and dispersion J-coupling values for sp^2 and sp^3 carbon sites, we performed a two-dimensional (2D) ^{13}C homonuclear double-quantum single-quantum (DQ-SQ) MAS experiment using the SC14 sequence[51]. This experiment allows the double quantum recoupling of dipolar-coupled spin-pairs and results in a 2D spectrum (with a direct SQ MAS dimension and an indirect DQ dimension for which the frequency corresponds to the sum of the two individual chemical shifts of the pair of coupled spins) allowing to trace out the C-C proximities between *both* inequivalent *and* equivalent sites. In the case of uniformly ^{13}C labeled samples, the DQ-SQ correlation spectra are dominated by the direct (one-bond) strong couplings due to dipolar truncation effects[51,70,71] and the longer-range C-C proximities are evidenced through indirectly correlated peaks of lower and negative intensities[51,54]. To avoid the presence of the indirectly correlated peaks and only observe correlation peaks reflecting the one-bond C-C strong coupling, we have used short DQ excitation and reconversion times (corresponding to two rotor periods) to record the 2D CP-filtered DQ-SQ correlation spectrum of the sample HC80, which has a high ^{13}C enrichment level. Cross-peaks (93.2-72.7 ppm) and (97.0-75.1 ppm) relate to the DQ excitation of C_1-C_2 groups in the α- and β-pyranose forms of glucose (whose presence was highly abundant also in the mother liquors). This is very important as glucose acts as the internal standard proving that the SC14 sequence under the employed conditions is selective to one C-C bond length.

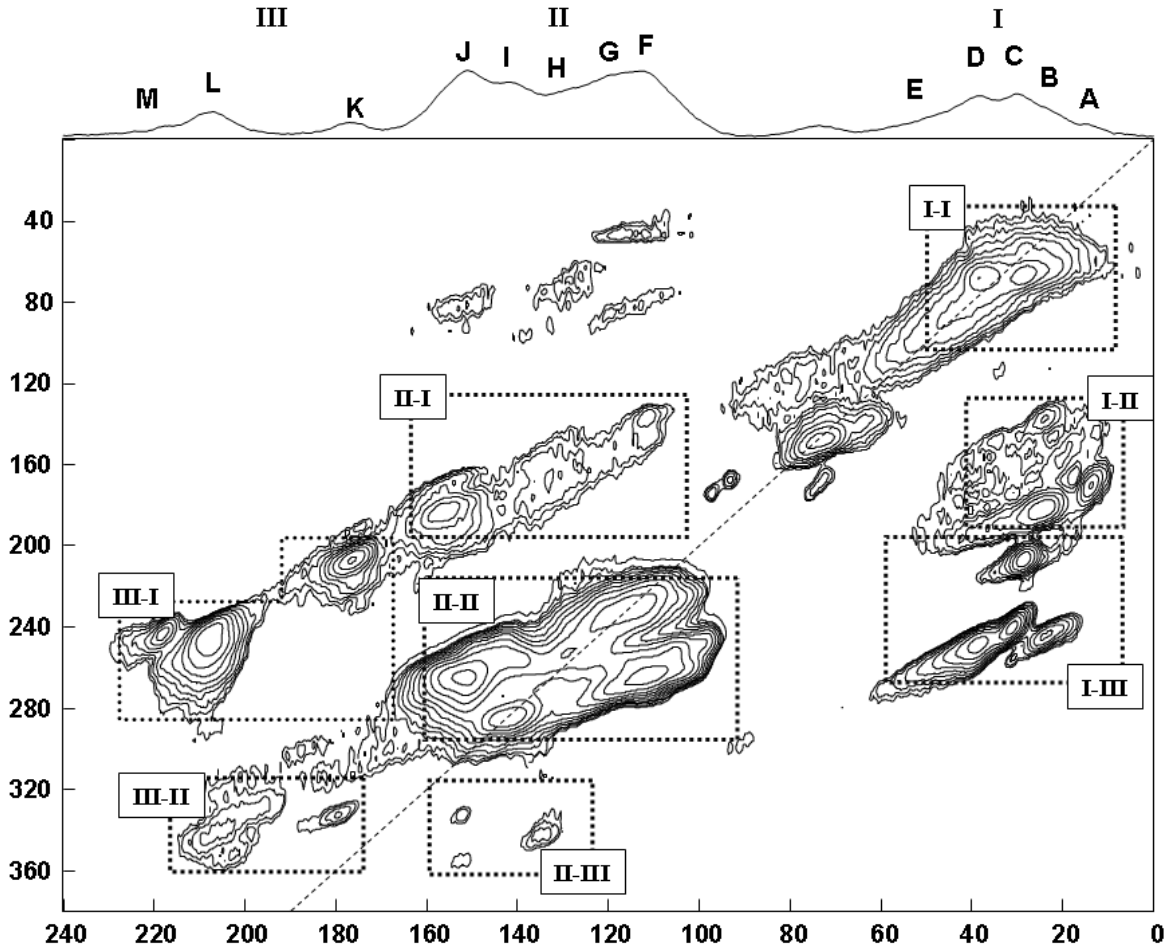

Figure 6 – 2D ^{13}C DQ-SQ MAS NMR correlation spectrum recorded on sample HC80 with τ_E=τ_R= 285.3 μs. Insights on the connectivity scheme are provided in Figure 4a,b-ESI

The main and most important result of the 2D DQ-SQ ^{13}C-^{13}C map is the visualization of the subtle connectivity among all species shown via the numerous cross-peaks and revealing the complexity of the carbon skeleton; however, they can be grouped in 5 different categories (symbolized by dashed rectangles in Figure 6), depending if they relate two carbon sites from the same spectral region (I-I and II-II) or from two different regions (I-II, I-III and II-III). The most intense correlation peaks belong to the II-II region, revealing strong homonuclear ^{13}C-^{13}C dipolar interactions between those sp^2 C sites. Peaks in the I-I region are less intense, but the dipolar coupling between sp^3 C is expected to be lower (longer C-C distance and possible internal mobility). As expected, no cross-peak relates two C=O sites from region III. Then, the most intense cross-peaks relating C sites from two different spectral regions are found in region I-III, showing

that the C=O groups are mostly bonded to sp^3 C sites. Fewer and less intense cross-peaks are found in regions I-II and II-III, suggesting the existence of spatially distinct domains that discriminate the sp^2 C sites from the others.

A closer look to the various regions will help proposing some structural motifs for the carbonaceous scaffold. For a clear trace of the connectivity on the 2D DQ-SQ map, one should refer to Figure 4-a,b-ESI.

- *Aromatic core* (*region II-II):* as established earlier by CP and INEPT experiments, region II corresponds primarily to α-substituted furanic rings where peak (F) originates from protonated β-carbons and peaks (I) and (J) are related to non-protonated α-carbons. For this spectral range, the DQ-SQ map shows four diagonal auto-correlation peaks (F-F, G-G, H-H and I-I) and three partly overlapping off-diagonal cross-correlation peaks (F-J), (F-I) and (G-J). The cross-correlation peaks (F-J) clearly suggest a connectivity between the α-carbons of two furanic rings through a C=C double bond, as shown in Scheme 2b, while the correlation peak (I-I) reveals a direct furanic connection as depicted in Scheme 2c. The auto- (G-G) and cross-correlation peaks (G-J) (F-B) indicate that quaternary β-carbons (F), (G) also constitute an important site for extra-furanic connectivity as shown in Scheme 2 d-f. To this regard, due to the equivalent amount of protonated and quaternary β-carbons (peaks F and G), as observed in SP MAS spectrum, one β-carbon out of two throughout the whole material is cross-linked. Finally, peak (H) at 131.2 ppm, given its chemical shift (typical for extended aromatic networks), its quaternary nature (as seen by CP behavior as a function of contact time) and the presence of an auto (H-H) cross peak (though of low intensity), describes the existence of spurious domains of grapheme sheets (Scheme 2a).

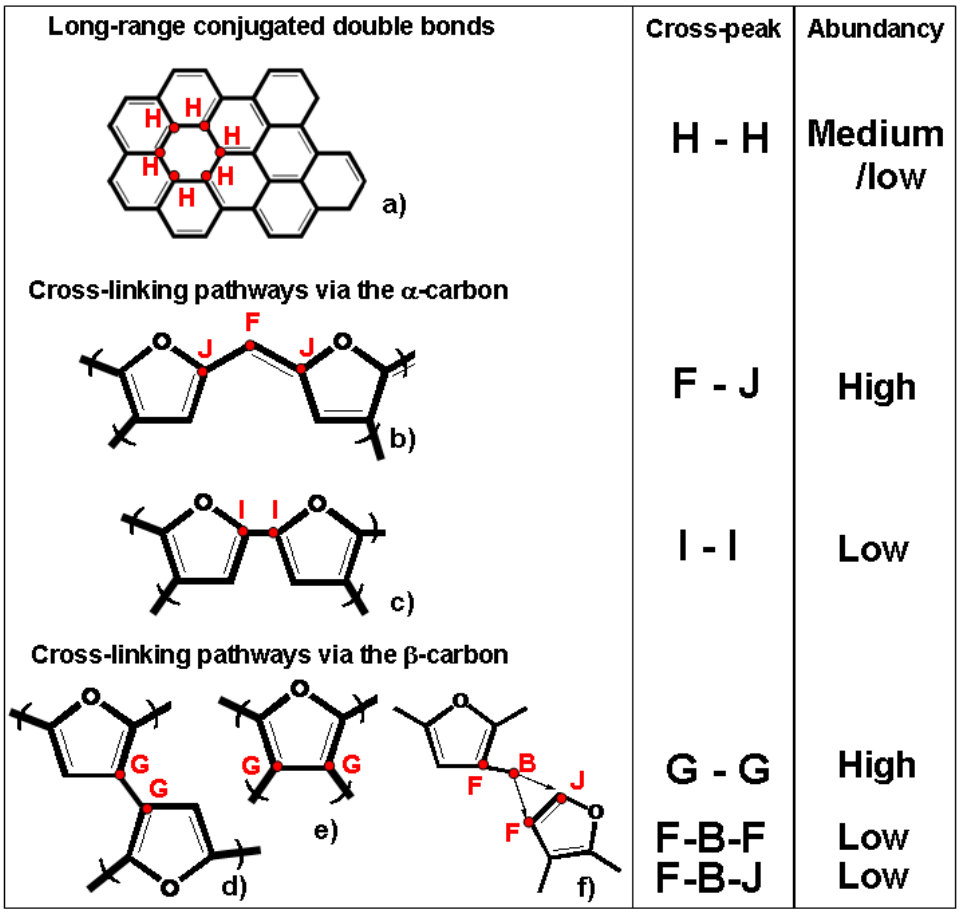

Scheme 2 - Structural motifs identified in region II-II from the 2D DQ-SQ ^{13}C-^{13}C correlation spectrum

Due to the intensity of the cross-peaks depicted in region II-II and the nature of the identified chemical species (Scheme 2), we believe that the core of the carbonaceous material is mainly composed of cross-linked furanic species. The chemical nature of the cross-links, spacers and possible end functions which are directly bonded to the furanic rings are described below after analyzing the correlation peaks between regions I-I, I-II, I-III and II-III.

- *Cross-links between furanic groups* (*Region II-I and II-III):* chemical functions which are directly connected to α-carbons are shown in Scheme 3 and are related to off-diagonal cross-peaks signals found in regions II-I and II-III of the DQ-SQ map of Figure 6. Signal (B) identifies a wide distribution of α- CH_2 groups, which can be in turn connected to either a second furan ring

(Scheme 3a) or to a carbonyl C=O group (signals M, Scheme 3b), which can be interpreted either as an aldedhyde or a ketone group connected to a (E) site at 50.5 ppm, most likely a CH group (see IRCP). At a lower extent, a carbonyl C=O group can be directly bound to α-carbons (Scheme 3c).

End functions: A low amount of direct functional groups directly linked to the furanic rings are also evidenced on the 2D correlation spectrum, as depicted in Scheme 3 d-f. Typically, aldehydic (Scheme 3d), methyl (Scheme 3e) and carboxy (Scheme 3f) groups bonded to the Cα carbon are evidenced through the off-diagonal (J-L), (J-A) and (J-K) cross-correlation peaks, respectively. Interestingly, the connection between the graphene-like (peak H) and the rest of the material is allowed by a keto group (cross-peak H-L).

Cross-linking pathways via the α-carbon	Cross-peak	Abundancy
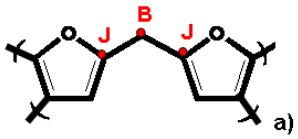 a)	B - J	High
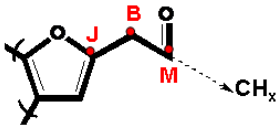 b)	J - B B - M M - E	High High Medium
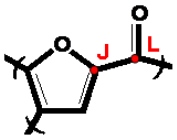 c)	J - L	Low
End functions at the α-carbon		
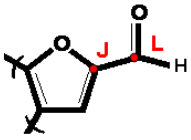 d)	J - L	Low
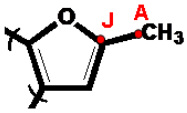 e)	J - A	Low
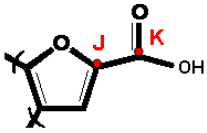 f)	J - K	Low

Scheme 3 - Cross-links between furanic rings and end functions at the α-carbon identified from the 2D DQ-SQ ^{13}C-^{13}C correlation spectrum

Cross-linking (Region III-I and I-I): These regions mainly show the interactions among carbons which compose the linkers between furanic moieties. Peak (B) identifies CH_2 (see IRCP) cross links between furanic species (peaks F and J): C_α-CH_2- C_α (J-B-J; high intensity), C_β-CH_2- C_β (F-B-F but very weak intensity), C_α-CH_2-C_β (J-B-F of weak intensity). Peak (E) at 50.5 ppm is a CH group according to IRCP experiments. The corresponding cross-peak is very broad and difficult to analyze, as it mainly connects to ketones (E-L) even if self CH-CH (E-E) or CH-CH_2 (E-D) correlation may also be possible.

Levulinic acid. All correlation peaks which have been discussed above are related to the structure of the furanic network. However, several additional intense cross-correlation peaks between region I and III are also clearly observed on the 2D correlation spectrum. This concern the (K-C) cross-correlation peaks at about 176.5 (K) and 28.7 (C) ppm in the SQ dimension, the (C-D) cross-correlation peak at 28.7 (C) and 38.3 (D) ppm, the (D-L) cross-correlation peaks at 38.3 (D) and 208 (L) ppm and finally a (L-C) correlation peaks at 208 (L) and 29.6 (C) ppm. Firstly, this set of correlation peak clearly indicates that the C peak contains two distinct components (which overlap completely in the 1D MAS and CP MAS spectra) with isotropic chemical shifts very similar to those of reported for the CH_3 (29.7 ppm) and CH_2 (27.9 ppm) groups of levulinic acid in $CDCl_3$ solution. Secondly, it evidences a K-C-D-L-C connectivity pattern which is characteristic of levulinic acid. The presence of levulinic acid was confirmed by an additional 2D ^{13}C homonuclear proton-driven magnetization exchange experiment realized with mixing time of 150 ms without the classical $\{^1H\}$-^{13}C CP step (result not shown). This approach allows the detection of all mobile species whose sensitivity is very low using a common CP approach due to molecular mobility. We were able to visualize the same connectivity pattern 29.6-210.0-38.3-28.7-176.5 ppm typical for the levulinic acid molecule. Meanwhile, sharps signals at 210.0 and 176.5 ppm which were lost after CP treatment were recovered and found to be coherent with peak attribution and connection related to levulinic acid. This additional experiment shows that part of LA exist in a free form within the material core.

One final remark: the four well-defined, but weak, cross-peaks at 75 ppm (marked by an asterisk) and (93, 97) ppm that can be attributed to the alpha and beta glucopyranose forms of glucose, as pointed out before and existing in spurious amounts (residual glucose was previously highlighted in mother liquors). It is clear from the 2D experiment that glucose does not correlate with any other carbon in the sample suggesting its simple entrapment in the carbonaceous matrix.

Discussion

All data support the idea that the main structural motif is the furan ring directly coming from HMF, the dehydration product of glucose. The very intense cross-peaks (J-F) provides the main spectroscopic evidence for this assumption: the amount of C=C-O and C=C is close to one-to-one. Any interpretation including widespread graphene sheets decorated with OH groups is not consistent with our data because an intense peak at 130 ppm, in addition to the resonance above 140 ppm, would be otherwise expected. This idea was also corroborated by the fact that direct carbonization of HMF provides a material whose chemical characteristics are very close to a glucose-synthesized carbon, as shown by previous solid state NMR experiments[29]. However the final products of thermally-treated biomass is not just a simple polyfurane, and the obtained material is quite complex, as suggested by the combination of co-existing structures depicted in schemes 2-3. Clearly, HMF units merge together mainly via α-carbons causing the long-range conjugated double bonded network but ramification from β-positions is also very common, as one β-carbon out of two is actually cross-linked. Interestingly, it is commonly accepted that carbon intermediates obtained from biomass pyrolisis at T< 350°C are constituted of a long-range aromatic network with terminal hydroxyl groups, which accounts for all NMR resonances between 110 and 150 ppm[25,31,32]. This interpretation, simply based on chemical shift assumptions from cross polarization experiments alone, is too loose to fit the whole set of our experimental data, which rely

on a number of complementary 1D and 2D techniques. Even if the presence of furan moieties in the structure of carbonaceous materials was very seldom highlighted, we believe that this is actually the only coherent explanation to our data. Given the very close similarity between ^{13}C NMR spectra of hydrothermally-treated glucose, polysaccharides[15,16] and pyrolyzed biomass[25,31,32], it is very likely that the initial stages of carbon formation goes through a cross-linked polyfuran network.

In order to have a picture of how the internal structure of the carbonaceous powder is disposed, one should consider several points: 1) dimension of each particle ranges between 0.5 and 5 μm[29]; 2) ^{13}C-^{13}C DQ-SQ experiments show that most of the furan rings are strongly mutually connected, suggesting their very close spatial proximity; 3) quantitative data indicate that a fairly high amount of carbon signal (> 20%, excluding free levulinic acid) comes from aliphatic carbons, and through-space connectivities show that most of those groups play a cross-linking role between carbonyls and furans. These considerations clearly exclude a long-range furanic network whose external surface is decorated with aliphatic chains and carbonyl groups but it rather leads us towards an interpretation in which the micrometer-sized carbon particle is actually composed of many interconnected (through short keto-aliphatic spacers) nano-sized domains in which an arbitrary combination of structures proposed in Scheme 2-3 co-exist together. The model as described above is visualized in Scheme 4.

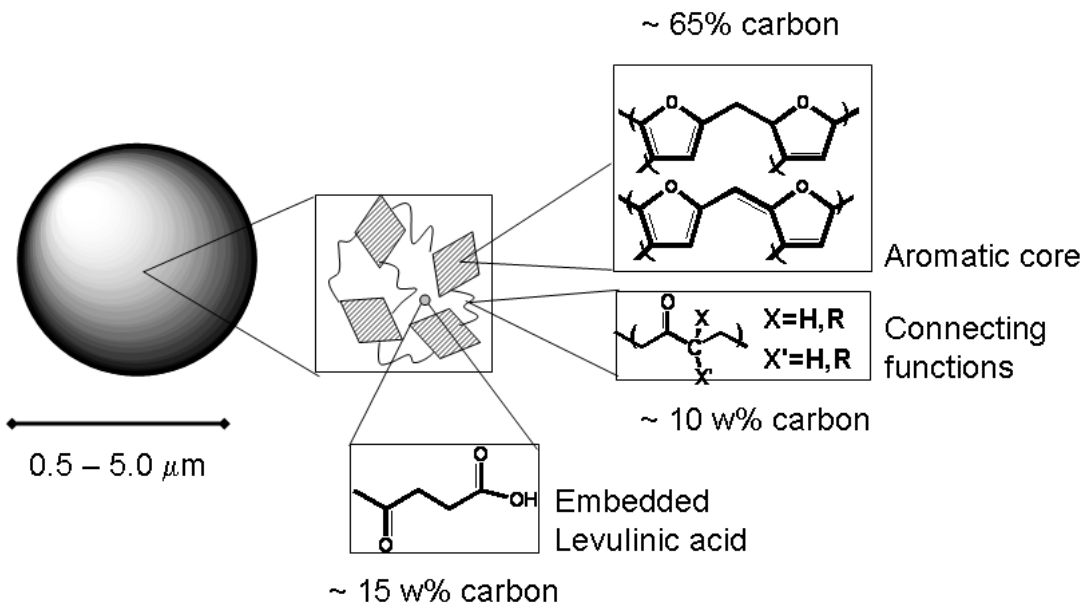

Scheme 4 – Structural model of carbon particles

Analysis of the overall intensity of the SP spectrum (Table 2) of HC80 let us attribute 13% of carbon to C=O containing groups, ca. 64% to sp^2 C=C carbons (in particular about 29% to α-carbons, 29% to β-carbons and 6% to graphene sheets) and around 23% to sp^3 carbons. When comparing these values to the carbonyl content both in glucose and HMF (16.6%), one can notice that the most carbonyl groups are kept throughout coalification. 66.6 % of sp^2 C=C carbons of HMF are practically kept unchanged during the process. This clearly proves that addition/polymerization of double bonds[72] as a leading coalification mechanism at least does not take place without consecutive elimination steps. On the other side, the 1:1 α-carbon to β-carbon ratio of HMF is nearly kept in the final material, which, once again, strongly supports the presence of the furan as main structural motif. The amount of the aliphatic part is in the end larger (23%) than in HMF (16.6%). Different mechanistic proposals can be made to account for the larger aliphatic contribution. Hydration of the aldehyde group of HMF may result in a further elimination of formic acid (this by-product is abundantly detected by GC-MS) and the consequent protonation of the C_α site as proved by INEPT experiments above (scheme 1); such a proton being very labile[73], a homo-condensation reaction forming a direct connection between two furan rings (see cross peak I-I in

Figure 6 and Scheme 2c) may occur. Formation of the abundant CH_2 groups acting as linkers between furan rings may originate from nucleophilic addition after possible elimination of the hydroxyl group on HMF. On the contrary, the nucleophilic attack on the aldehyde group of HMF from a second furanic unit may lead to hydroxyl species which can in turn be eliminated with subsequent electron rearrangement and formation of a sp^2 CH carbon between two furan moieties (scheme 2b). The formation of specific CH_3 and COOH ending groups (from Cα of furan ring) was previously reported[73] (scheme 3 e-f) while some doubts still exist on the attribution and explanation of the CH group at 50.5 ppm (E). According to the DQ-SQ map, its direct connection to ketone groups has the highest probability (even CH-CH or CH-CH_2 bonds may exist at a minor extent). In this case, a reaction path directing towards a bridging CH between three C=O groups (this could be justified by the broadness of the E band) may not be excluded. In fact, cyclic condensation of the levulinic acid (LA) can lead to cyclic diketone species having a linking CH_2 site to which a third LA molecule could react via an aldol condensation step. Further insights can probably be found in the complex chemistry of furans, as largely described and commented in reference 73.

Conclusion

In this communication we tried to address the difficult problem of the structure resolution of amorphous carbonaceous materials obtained, here, from hydrothermal carbonization processing of biomass. Based on previous comparative studies, glucose was selected as a good model carbon source since it allows the preparation of ^{13}C enriched samples and thus the use of solid-state ^{13}C NMR to investigate the chemical composition and local structure of the hydrothermally treated materials. Several standard MAS NMR techniques (SP, CP, IRCP), which are mainly used in the study of carbon structures, have been used here to identify the amount and type of sp^2 and sp^3 carbon sites. In addition, we used through-bond filtering techniques based on J-coupling (INEPT), which provided a clear-cut distinction between protonated and quaternary carbons. Finally, the connectivity between carbon species was identified using a 2D ^{13}C-^{13}C correlation experiment based on double quantum excitation of through-space dipolar-coupled nuclei.

We found that about 60% of the carbon atoms belong to a cross-linked furan-based structure. Furan moieties are either directly linked via the alpha carbon or via sp^2 or sp^3 type carbon groups, where cross-linking can occur. Additional cross-linking sites are located at the beta carbons of the furan ring. Interestingly, we found that levulinic acid, one of the decomposition product of hydroxymethylfurfural (HMF), is highly abundant in the final material both as embedded molecule and as copolymerized compound. A clear set of CP-blind NMR signals can be related to free molecular levulinic acid (also corroborated with ^{13}C-^{13}C exchange spectroscopy experiments) while the 2D ^{13}C-^{13}C DQ-SQ map suggests levulinic acid copolymerizes with the polyfuran network.

We believe that such a complex structure is the result of a cascade of coexisting reactions paths of inter-furfural polymerization and aldol-condensation reactions involving both the furan motif and dehydrated glucose-based products, like levulinic acid. This more vinylic, aliphatic structure explains many of the properties of hydrothermal coal, such as rather high combustion value, high chemical reactivity, reductive properties, and high ion binding capacity and wettability. In the end, we can provide a pictorial image of the inner carbon structure obtained via hydrothermal treatment of glucose but which can be extended to depict more carbons obtained from more complex biomass both via a hydrothermal and a pyrolysis step. Interestingly, comparing these results with literature studies, it seems that the furan ring may be the actual carrying structural motif for biomass-derived carbons obtained at pyrolysis temperatures below 350°C, in contrast with many previous reports in which the existence of oxydized graphene sheets was supposed. Here, less than 6% of all carbons are involved in such a structural motif.

Acknowledgements

We thank Prof. M. Sollogoub (IPCM, Université Pierre et Marie Curie, Paris, France) for helpful discussions.

References

[1] Titirici, M.-M.; Thomas, A.; Antonietti, M. *New J. Chem*. **2007**, *31*, 787

[2] Titirici, M.-M.; Thomas, A.; Antonietti, M. *Adv. Funct. Mater.* **2007**, *17*, 1010

[3] Titirici, M.-M.; Thomas, A.; Yu, S.-H.; Muller, J.-O.; Antonietti, M. *Chem. Mater*. **2007**, *19*, 4205

[4] Budarin, V.; Clark, J. H.; Hardy, J. J. E.; Luque, R.; Milkowski, K.; Tavener, S. J.; Wilson, A. J. *Angew. Chem. Int. Ed*. **2006**, *45*, 3782

[5] Demir-Cakan, R.; Baccile, N.; Antonietti, M.; Titirici, M.-M. *Chem. Mater*. **2009**, DOI: 10.1021/cm802141h

[6] Corma, A.; Iborra, S.; Velty, A. *Chem. Rev*. **2007**, *107*, 2411

[7] Qian, H.-S.; Yu, S.-H.; Luo, L.-B.; Gong, J.-Y.; Fei, L.-F.; Liu, X.-M. *Chem. Mater*. **2006**, *18*, 2102

[8] Qian, H.-S.; Antonietti M.; Yu S.-H. *Adv. Funct. Mater.* **2007**, *17*, 637

[9] Titirici, M.-M.; Thomas, A.; Antonietti, M. *J. Mater. Chem*. **2007**, *17*, 3412

[10] Budarin, V.; Luque, R.; Macquarrie, D. J.; Clark, J. H. *Chem. Europ. J*. **2007**, *13*, 6914

[11] Budarin, V. L.; Clark, J. H. ; Luque, R. ; Macquarrie, D. J. *Chem. Commun*. **2007**, 634

[12] Lourvanij, K.; Rorrer, G. L. *Appl. Catal., A* **1994**, *109*, 147

[13] Lourvanij, K.; Rorrer, G. L. *Ind. Eng. Chem. Res*. **1993**, *32*, 11

[14] Antal, M. J.; Mok, W. S. L.; Richards, G. N. *Carbohyd. Res*. **1990**, *199*, 91

[15] Yao, C.; Shin, Y.; Wang, L.-Q.; Windisch, C. F. Jr.; Samuels, W. D.; Arey, B. W.; Wang, C.; Risen, W. M. Jr.; Exarhos, G. J. *J. Phys. Chem. C* **2007**, *111*, 15141

[16] Sun, X.; Li, Y. *Angew. Chem.* **2004**, *116*, 607

[17] Barron, P. F.; Wilson, M. A. *Nature* **1981**, *289*, 275

[18] Sullivan, M. J.; Maciel, G. E. *Anal. Chem.* **1982**, *54*, 1608

[19] dela Rosa, L.; Pruski, M.; Lang, D.; Gerstein, B.; Solomon, P. *Energy & Fuels* **1992**, *6*, 460

[20] Tekely, P.; Nicole, D.; Brondeau, J.; Delpuech, J.-J. *J. Phys. Chem.* **1986**, *90*, 5608

[21] Lukins, P. B.; McKenzie, D. R.; Vassallo, A. M.; Hanna, J. V. *Carbon*, **1993**, *31*, 569

[22] Azami, K.; Yamamoto, S.; Sanada, Y. *Carbon*, **1993**, *31*, 611

[23] Fu, F.; Liu, L.; Huang, W.; Sun, P. *J. Appl. Polym. Sci*., **2003**, *87*, 2253

[24] Kawashima, H.; Yamada, O. *Fuel Proc. Tech.* **1999**, *61*, 279

[25] Sharma, R. K.; Wooten, J. B.; Baliga, V. L.; Hajaligol, M. R. *Fuel* **2001**, *80*, 1825

[26] Sharma, R. K.; Wooten, J. B.; Baliga, V. L.; Martoglio-Smith, P. A.; Hajaligol, M. R. *J. Agric. Food Chem.* **2002**, *50*, 771

[27] Holtman, K. M.; Chang, H.-M.; Jameel, H.; Kadla, J. F. *J. Wood Chem. Tech*. **2006**, *26*, 21

[28] Bardet, M.; Hediger, S.; Gerbaud, G.; Gambarelli, S.; Jacquot, J. F.; Foray, M. F.; Gadelle, A. *Fuel* **2007**, *86*, 1966

[29] Titirici, M.-M.; Antonietti, M.; Baccile, N, *Green Chem.* **2008**, *10*, 1204

[30] Freitas, J. C. C.; Bonagamba, T. J.; Emmerich, F. G. *Carbon* **2001**, *39*, 535

[31] Zhang, X.; Golding, J.; Burgar, I. *Polymer* **2002**, *43*, 5791

[32] Wooten, J. B.; Seeman, J. I.; Hajaligol, M. R. *Energy Fuels* **2004**, *18*, 1

[33] Cai, W.; Piner, R. D.; Stadermann, F. J.; Park, S.; Shaibat, M. A.; Ishii, Y.; Yang, D.; Velamakanni, A.; An, S. J.; Stoller, M.; An, J.; Chen, D.; Ruoff, R. F. *Science* **2008**, *321*, 1815

[34] Bennett, A. E.; Rienstra, C. M.; Auger, M; Lakshmi, K. V.; Griffin, R. G. *J. Chem. Phys.* **1995**, *103*, 6951

[35] Massiot, D.; Fayon, F.; Capron, M.; King, I.; Le Calve, S.; Alonso, B.; Durand, J.-O.; Bujoli, B.; Gan, Z.; Hoatson, G. *Magn. Reson. Chem*. **2002**, *40*, 70.

[36] Hediger S.; Meier, B.H.; Kurur, N.D.; Bodenhausen, G.; Ernst, R.R. *Chem. Phys. Lett.* **1994**, *223*, 283

[37] Hediger, S.; Meier, B.H.; Ernst, R.R., *Chem. Phys. Lett.* **1995**, *240*, 449

[38] Christiansen, S.C.; Hedin, N.; Epping, J.D.; Janicke, M.T.; del Amo, Y.; Demarest, M.; Brzezinski, M.; Chmelka, B.F. *Sol. St. Nucl. Magn. Res.* **2006**, *29*, 170

[39] Cory, D. G.; Ritchey, W. M. *Macromol.* **1989**, *22*, 1611

[40] Tekely, P.; Montigny, F.; Canet, D.; Delpuech, J. J. *Chem. Phys. Lett*. **1990**, *175*, 401.

[41] Wu, X.; Zilm, K. W. *J. Magn. Reson*. **1993**, *A102*, 205.

[42] Palmas, P.; Tekely, P.; Canet, D. *J. Magn. Reson*. **1993**, *A104*, 26.

[43] Babonneau, F.; Maquet, J.; Bonhomme, C.; Richter, R.; Roewer, G.; Bahloul, D. *Chem. Mater*. **1996**, *8*, 1415

[44] Wu, X.; Zhang, S. *Chem. Phys. Lett*. **1989**, *156*, 79.

[45] Alemany, L. B.; Grant, D. M.; Pugmire, R. J.; Alger, T. D.; Zilm, K. W. *J. Am. Chem. Soc*. **1983**, *105*, 2142

[46] Morris, G. A.; Freeman, R. *J. Am. Chem. Soc*. **1979**, *101*, 760-762

[47] Burum, D. P.; Ernst, R. R. *J. Magn. Reson*. **1980**, *39*, 163

[48] Fyfe, C. A.; Wong-Moon, K. C.; Huang, Y.; Grondey, H. *J. Am. Chem. Soc*. **1995**, *117*, 10397

[49] Alonso, B.; Massiot, D. *J. Magn. Reson*. **2003**, *163*, 347

[50] Elena, B.; Lesage, A.; Steuernagel, S.; Boeckmann, A.; Emsley, L. *J. Am. Chem. Soc*. **2005**, *127*, 17296

[51] Brinkmann, A.; Edén, M.; Levitt, M. H. *J. Chem. Phys.*, **2000**, *112*, 8539

[52] Lee, Y. K.; Kurur, N. D.; Helmle, M.; Johannessen, O.; Nielsen, N. C.; Levitt, M. H. *Chem. Phys. Lett.* **1995**, *242*, 304

[53] Hohwy, M.; Jakobsen, H. J.; Edén, M.; Levitt, M. H.; Nielsen, N. C. *J. Chem. Phys.* **1998**, *108*, 2686.

[54] Hohwy, M.; Rienstra, C.M.; Jaroniec, C. P.; Griffin, R. G. *J. Chem. Phys.* **1999**, *110*, 7983

[55] States, D. J.; Haberkorn, R. A.; Ruben, D. J. *J. Magn. Reson.* **1982**, *48*, 286

[56] Baccile, N.; Laurent, G.; Bonhomme, C.; Innocenzi, P.; Babonneau, F. *Chem. Mater.* **2007**, *19*, 1343

[57] Meier, B. H. Advances in Magnetic and optical Resonance, vol. 18, 1, Warren W.S. Ed., Academic Press, New York, **1994**.

[58] Schmidt-Rohr, K.; Spiess, H. W. *Multidimensional Solid-State NMR and Polymers*; p.431 Academic Press: San Diego, **1994**.

[59] Szeverenyi, N. M.; Sullivan, M. J.; Maciel, G. E. *J. Magn. Res*. **1982**, *47*, 462

[60] Ulbricht, R. J.; Northup, S. J.; Thomas, J. A. *Fund. Appl. Toxic*. **1984**, *4*, 843

[61] Lourvanij, K.; Rorrer, G. L. *Ind. Eng. Chem. Res*. **1993**, *32*, 11

[62] Lourvanij, K.; Rorrer, G. L. *App. Catal. A: General* **1994**, *109*, 14

[63] Asghari, F. S.; Yoshida, H. *Ind. Eng. Chem. Res*. **2006**, *45*, 2163

[64] Spectral Database for Organic Compounds, SDBS, National Institute of Advanced Industrial Science and Technology (AIST), Japan

[65] Girisuta, B.; Janssen, L. P. B. M.; Heeres, H. J. *Chem. Eng. Res. Des*., **2006**, *84*, 339

[66] Alemany, L. B.; Grant, D. M.; Pugmire, R. J.; Alger, T. D.; Zilm, K. W. *J. Am. Chem. Soc*., **1983**, *105*, 2133; Alemany, L. B.; Grant, D. M.; Pugmire, R. J.; Alger, T. D.; Zilm, K. W. *J. Am. Chem. Soc*., **1983**, *105*, 2142

[67] Lesage, A.; Auger, C.; Caldarelli, S.; Emsley, L. *J. Am. Chem. Soc*., **1998**, *120*, 9059

[68] Lesage, A.; Bardet, M.; Emsley, L. *J. Am. Chem. Soc*., **1999**, *121*, 10987

[69] Ishii, Y. *J. Chem. Phys*., **2001**, *114*, 8473

[70] Hohwy, M.; Rienstra, C. M.; Griffin, R. G. *J. Chem. Phys.* **2002**, *117*, 4973

[71] Grommek, A.; Meier, B. H.; Ernst, M. *Chem. Phys. Lett.* **2006**, *427*, 404

[72] Note: diene polymerization would reduce the number of double bonds to 33 %, while 4 + 2 cycloadditions would result in 50% sp^2-content.

[73] Gandini, A.; Belgacem, M. N. *Prog. Polym. Sci*. **1997**, 22, 1203